AGU PUBLICATIONS

JGR

Journal of Geophysical Research: Atmospheres

RESEARCH ARTICLE
10.1002/2016JD025541

Key Points:
- Dust storms result in increased concentrations but decreased solubility for most aerosol trace elements
- Both the concentrations and speciation patterns of dissolved trace elements in cloud water are highly pH dependent
- Aerosol-cloud interactions significantly influence the speciation, solubilization, and scavenging of atmospheric trace elements

Supporting Information:
- Supporting Information S1
- Table S1
- Movie S1
- Movie S2

Correspondence to:
Y. Wang,
wy@sdu.edu.cn

Citation:
Li, T., Y. Wang, J. Zhou, T. Wang, A. Ding, W. Nie, L. Xue, X. Wang, and W. Wang (2017), Evolution of trace elements in the planetary boundary layer in southern China: Effects of dust storms and aerosol-cloud interactions, *J. Geophys. Res. Atmos.*, *122*, 3492-3506, doi:10.1002/2016JD025541.

Received 19 JUN 2016
Accepted 27 FEB 2017
Accepted article online 2 MAR 2017
Published online 24 MAR 2017

Evolution of trace elements in the planetary boundary layer in southern China: Effects of dust storms and aerosol-cloud interactions

Tao Li[1], Yan Wang[1], Jie Zhou[2], Tao Wang[3,4], Aijun Ding[5], Wei Nie[3,5], Likun Xue[3], Xinfeng Wang[3], and Wenxing Wang[3]

[1]School of Environmental Science and Engineering, Shandong University, Jinan, China, [2]Shandong Provincial Environmental Information and Monitoring Centre, Jinan, China, [3]Environment Research Institute, Shandong University, Jinan, China, [4]Department of Civil and Environmental Engineering, Hong Kong Polytechnic University, Hong Kong, [5]Institute for Climate and Global Change Research and School of Atmospheric Sciences, Nanjing University, Nanjing, China

Abstract Aerosols and cloud water were analyzed at a mountaintop in the planetary boundary layer in southern China during March–May 2009, when two Asian dust storms occurred, to investigate the effects of aerosol-cloud interactions (ACIs) on chemical evolution of atmospheric trace elements. Fe, Al, and Zn predominated in both coarse and fine aerosols, followed by high concentrations of toxic Pb, As, and Cd. Most of these aerosol trace elements, which were affected by dust storms, exhibited various increases in concentrations but consistent decreases in solubility. Zn, Fe, Al, and Pb were the most abundant trace elements in cloud water. The trace element concentrations exhibited logarithmic inverse relationships with the cloud liquid water content and were found highly pH dependent with minimum concentrations at the threshold of pH ~5.0. The calculation of Visual MINTEQ model showed that 80.7–96.3% of Fe(II), Zn(II), Pb(II), and Cu(II) existed in divalent free ions, while 71.7% of Fe(III) and 71.5% of Al(III) were complexed by oxalate and fluoride, respectively. ACIs could markedly change the speciation distributions of trace elements in cloud water by pH modification. The in-cloud scavenging of aerosol trace elements likely reached a peak after the first 2–3 h of cloud processing, with scavenging ratios between 0.12 for Cr and 0.57 for Pb. The increases of the trace element solubility (4–33%) were determined in both in-cloud aerosols and postcloud aerosols. These results indicated the significant importance of aerosol-cloud interactions to the evolution of trace elements during the first several cloud condensation/evaporation cycles.

1. Introduction

Trace elements in the atmosphere that are derived from natural processes or emitted by human activities can adversely affect on human health [*Fomba et al*., 2013] and can be transported over hundreds or even thousands of kilometers by virtue of their residence times of days, considerably contributing to transboundary environment pollution [*Travnikov et al*., 2012]. More importantly, once lofted into the upper planetary boundary layer or even the free troposphere, where clouds or fogs frequently occur, transition metals can play significant roles in heterogeneous/multiphase chemistry, free radical budgets, generation of sulfate, and degradation of organics in atmospheric aqueous phases (e.g., cloud drops and aqueous aerosols) [*Deguillaume et al*., 2005; *Harris et al*., 2013; *Herrmann et al*., 2015; *Mao et al*., 2013; *Weller et al*., 2014; *Weschler et al*., 1986].

Accumulation mode particles can act as cloud condensation nuclei (CCN) and determine the chemical composition of cloud water including major ions and trace elements [*Plessow et al*., 2001]. The numerous aerosol particles in the planetary boundary layer have many opportunities to encounter or interact with clouds and influence each other, that is, aerosol-cloud interactions (ACIs), which have very complicated effects on tropospheric chemical processes [*Ervens*, 2015], the physical and chemical properties of aerosols, clouds and trace gases in the troposphere [*Eck et al*., 2012; *Lihavainen et al*., 2010; *Unger et al*., 2009], and eventually the climate system through radiative forcing [*Rosenfeld et al*., 2014]. It has been estimated that the elevated aerosol concentrations can lead to an increase of 5% in the global average cloud cover [*Kaufman and Koren*, 2006]. Recent studies showed that anthropogenic aerosol particles from ship effluent can remarkably impact cloud properties in ship track regions, e.g., higher cloud optical thickness, smaller cloud droplet size, and elevated liquid water content (LWC), than clean regions [*Possner et al*., 2015; *Russell et al*., 2013], along with higher

cloud acidity and concentrations of sulfate, nitrate, and trace elements [*Wang et al*., 2014]. Simultaneously, cloud processes can modify aerosol particles. Bimodal sizes in the accumulation mode with higher aerosol optical depth are often observed in cloud-processed aerosols by retrieved Aerosol Robotic Network data and in situ measurements [*Eck et al*., 2012], and new particle formation has occurred in clouds according to aircraft measurements [*Lee*, 2004].

The concentrations and sources of trace elements in fog or cloud water have been investigated in many different regions of North America [*Hutchings et al*., 2008; *Malcolm et al*., 2003; *Straub et al*., 2012; *Wang et al*., 2014], Europe [*Cini et al*., 2002; *Fomba et al*., 2015; *Plessow et al*., 2001], and Asia [*Ghauri et al*., 2001; *Liu et al*., 2012; *Sun et al*., 2015]. *Graedel et al*. [1985] suggested the significant influence of transition metal complexes on atmospheric droplet acidity and free radical formation, so knowledge of the chemical speciation of trace elements in field observations is very crucial. The oxidation states of trace metals (e.g., Fe, Cu, and Mn) were measured to evaluate their roles in atmospheric aqueous phase chemistry [*Parazols et al*., 2006; *Siefert et al*., 1998]. The flight observation during the E-PEACE Campaign proved that Fe(II)/Fe(III) redox cycling was likely to cause the photolysis of oxalate in cloud drops [*Sorooshian et al*., 2013]. Trace metals in aerosols and clouds were closely studied in the field campaign HCCT-2010 at Mount Schmücke, which investigated aerosol-cloud interactions [*Fomba et al*., 2015]. Thus, the catalysis of transition metal ions has been confirmed to be an important in-cloud oxidation pathway of SO_2 in sulfur isotope experiments [*Harris et al*., 2013]. The chemical equilibrium model is an efficient and convenient approach to determine the complexation of trace elements in atmospheric aqueous phase [*Scheinhardt et al*., 2013; *Siefert et al*., 1998; *Sun et al*., 2015] in the context of knowing almost all the composition contents. The simulations by *Weller et al*. [2014] indicated that Fe(III) was mainly coordinated by oxalate and the complex photolysis could be a considerable sink process of carboxylic acids in clouds. However, the chemical reaction mechanisms of trace metals in atmospheric multiphase are still unknown because many properties, such as the dissolution kinetics and complexation in realistic clouds, remain poorly understood [*Deguillaume et al*., 2005].

Aerosol particles are the only source of trace elements in cloud water and typically undergo about 10 condensation/evaporation cloud cycles before removal [*Warneck*, 1999]. But the behaviors of trace elements during aerosol-cloud interaction events are far from clearly known. Therefore, learning the characteristics and evolution of trace elements in aerosols and droplets is essential and critical to improve our understanding of the effects of trace elements on the atmospheric composition and chemistry.

This study presents the concentrations, solubility, and chemical speciation of trace elements in aerosols and clouds at the top of Mount Heng in southern China during the spring of 2009. The effects of dust storms, cloud water acidity, and aerosol-cloud interactions on the chemical evolution of trace elements in both aerosols and cloud water are discussed.

2. Experiments and Methods

2.1. Site Description

The observation site was at the summit of Mount Heng (27°18′N, 112°42′E, 1269 m above sea level) in Hunan Province, southern China (Figure S1 in the supporting information). The summit of Mount Heng is located in the planetary boundary layer, where cloud events frequently occur because of the continual encounter of cold and warm airflow in spring [*Sun et al*., 2010]. Therefore, this location is a favorable platform to observe ACI events and the long-range transport of air pollutants or dust. Although very few local anthropogenic emissions occur at Mount Heng, which is a national nature reserve, the intensive nonferrous industries in the Chang-Zhu-Tan city clusters, which are situated in central Hunan Province approximately 70 km to the north of Mount Heng, may contribute to air pollution at the observation site.

2.2. Observation Campaign

The observation campaign was conducted from 11 March to 31 May in 2009. Daily TSP (total suspended particulates) and $PM_{2.5}$ (particulate matter with an aerodynamic diameter of 2.5 μm or less) samples were manually collected on preheated (500°C) microquartz fiber filters (90 mm, Munktell, Switzerland) during clear days. Two particulate matter samplers (TH-150A, Tianhong Co., China), one with a TSP impactor and another with a $PM_{2.5}$ series impactor, were employed at a flow rate of 100 L min^{-1}. Aerosol samples were intensively collected every 4–12 h during dust storms. The sample filters were then saved at –20°C in the dark for

laboratory analysis. The details of this cloud water sampling procedure were described by *Sun et al*. [2010]. In brief, cloud water samples were collected via a single-stage Caltech Active Strand Cloudwater Collector and then immediately filtered and preserved at 4°C after field measurement of conductivity and pH values.

Continuous aerosols and trace gases were measured by using the following instruments as presented by *Nie et al*. [2012]: TEOM (Thermo Electron Corporation, East Greenbush, NY, USA) for measuring the hourly PM_{10} and $PM_{2.5}$, TEI Model 43C for SO_2, and TEI Model 42CY for NO_y. The meteorology data were provided by the Mount Heng Meteorological Station.

2.3. Pretreatment and Chemical Analysis

The extraction procedure of aerosol particle samples that was employed in this study was the same as that in *Li et al*. [2015]. Generally, half of the sample filters were extracted in pure water for 1 h by using ultrasonic vibrations to extract water-soluble ions and soluble trace elements. A quarter of the sample filters, acid mixture (65% HNO_3 and 30% H_2O_2), sealed Teflon vessels, and a microwave digestion system were used to digest the total fractions of aerosol trace elements.

Water-soluble ions in the aerosol and cloud water samples, including Na^+, NH_4^+, K^+, Mg^{2+}, Ca^{2+}, F^-, Cl^-, NO_2^-, SO_4^{2-}, and NO_3^- were analyzed by ion chromatography (Dionex, ICS-90) [*Sun et al*., 2010]. The concentrations of small carboxylic acid ions (formate, acetate, oxalate, lactate, propionate, and mesylate) in cloud water were determined by using ion chromatography (Dionex, ICS-2500) [*Y. Wang et al*., 2011]. The total and water-soluble trace elements in the aerosols and dissolved trace elements in the cloud water, including Al, V, Cr, Mn, Fe, Ni, Cu, Zn, As, Se, Mo, Cd, Sb, Ba, and Pb were measured by inductively coupled plasma–mass spectrometry (ICP-MS, Agilent 7500a) based on the EPA 200.8 method.

2.4. Chemical Speciation Calculation

The chemical speciation of dissolved trace elements in cloud water was calculated by the Visual MINTEQ 3.0 model (http://vminteq.lwr.kth.se) considering the difficulties of direct determination. Visual MINTEQ is a chemical equilibrium model that was developed to calculate metal speciation in natural waters. The field pH values and liquid phase concentrations of water-soluble ions, small carboxylic acid ions, and trace elements (Fe, Al, Zn, Pb, and Cu) of 188 cloud water samples were used as input parameters (see the data set in Table S1). Thus, the percentage distribution of dissolved trace metal speciation was obtained.

In this study, the ionic strength I was calculated based on the concentrations of ions measured in cloud water. As shown in Table S1, the cloud water samples were dilute solutions with ionic strengths from 10^{-5} to 10^{-2} M. Then, the activity coefficients γ were estimated using the Davies equation, which is applicable at ionic strengths below 0.5 M:

$$\log\gamma_i = -Az_i^2\left(\frac{\sqrt{I}}{1+\sqrt{I}} - 0.3I\right)$$

where $A = 1.82\times10^6(\varepsilon T)^{-3/2}$ (ε is the dielectric constant) and T was set to 13.4°C, the mean temperature of cloud water.

The oxidation states of trace elements could not be distinguished by ICP-MS. Zn, Pb, and Cu were assumed to be present in +II oxidation states and Al in +III, which are their predominant states in aqueous solutions. However, the iron oxidation states +II and +III greatly vary in atmospheric liquid phases [*Deguillaume et al*., 2005], and only the total Fe concentration was measured here. However, we found that the Fe(II)/Fe(III) ratios barely changed their speciation distribution as a function of pH (see Text S1 for details), which is the main research topic in this study. The equivalent amount of Fe(II) and Fe(III) was chosen as the best guess to calculate the speciation of dissolved iron. Chemical equilibria in solid phases and photoredox reactions during the daytime and nighttime were not considered here.

2.5. Scavenging Ratio Calculation

Nucleation scavenging is usually more efficient to remove particles that act as CCN and most chemical species therein (mass scavenging > 90%) from the troposphere [*Ervens*, 2015], and coarse aerosols are preferentially removed via cloud impaction scavenging or gravity sedimentation [*Warneck*, 1999]. Thus, the $PM_{2.5}$ samples were selected to determine the scavenging effects on aerosol particles and trace elements by using

different approaches in this study. According to the continuous $PM_{2.5}$ data, the cloud mass scavenging ratios (F) for aerosol particles were calculated as

$$F = \frac{C_{clear} - C_{int}}{C_{clear}}$$

where C_{clear} and C_{int} are the concentrations in clear air and cloud interstitial space, respectively.

Based on the availability of precloud aerosols and cloud water concentrations, the mass scavenging ratios (ε) for aerosol trace elements were estimated from the following relationship by *Junge* [1963]:

$$\varepsilon = C_c \times \mathrm{LWC}/C_a$$

where C_c and C_a represent the concentration of a species in cloud water ($\mu g\,L^{-1}$) and fine aerosol particles ($ng\,m^{-3}$), respectively. The formula is particularly applicable to the nucleation scavenging of submicron particles which comprise most of the aerosol mass.

3. Results and Discussion

3.1. Overview of Dust Storms and ACI Events

Figure 1 displays the time series of manual aerosol and cloud water samples, continuous aerosols, and trace gases, and meteorological parameters at Mount Heng throughout the observation period. Overall, 43 TSP (coarse) and 38 $PM_{2.5}$ (fine) aerosol samples and 192 cloud water samples were manually collected. A nationwide intense Asian dust storm on 24–26 April and a moderate floating dust storm on 22–23 March were captured at Mount Heng, which were also observed at Mount Hua, Mount Tai [*G. Wang et al.*, 2011], Chengdu [*Tao et al.*, 2013], Hong Kong, and Taiwan [*Wong et al.*, 2015]. During these dust periods, a prevailing northerly wind occurred with wind speeds below $5\,m\,s^{-1}$ and relative humidity (RH) as low as 40%. The pollution gases SO_2 and NO_y both increased by 6–9 ppb during the dust storms and were likely entrained during the long-range transport through the industrialized eastern and central China. The concentrations of major ions (except NH_4^+), such as SO_4^{2-}, NO_3^-, and Ca^{2+}, significantly increased by approximately 2 to 6 times, which was consistent with the sharply elevated coarse and fine aerosols. A more detailed discussion of the mass concentrations of aerosols and water-soluble ions during nondust and dust storm periods can be found in Text S2 in the supporting information [*Tao et al.*, 2013; *G. Wang et al.*, 2011].

The cloud periods were characterized by high relative humidity (RH more than 95%) and weak solar radiation (below $400\,W\,m^{-2}$), when extremely low concentrations of continuous PM_{10} and $PM_{2.5}$ were usually observed because of the cloud scavenging of aerosol particles. The LWC of cloud water ranged from 0.03 to $0.47\,g\,m^{-3}$, and the pH values varied between 2.91 and 6.91 with a volume-weighted mean (VWM) pH value of 3.80. Five ACI events are shown in Figure S3, and the dust ACI events were confirmed by the dust-cloud migrations in Movies S1 and S2, the Moderate Resolution Imaging Spectroradiometer true color images, and CALIPSO vertical mask in Figure S4.

3.2. Effects of Dust Storms on Aerosol Trace Elements

The aerosol trace elements concentrations at Mount Heng are listed in Table 1. Fe was the most predominant trace element in both fine and coarse aerosols at Mount Heng during nondust periods, followed by Al and Zn, but their concentrations were obviously lower than those at Mount Tai in the North China Plain [*Deng et al.*, 2011]. High concentrations of toxic Pb ($108.6\,ng\,m^{-3}$), As ($21.1\,ng\,m^{-3}$), and Cd ($5.55\,ng\,m^{-3}$) in fine aerosols were observed at Mount Heng, which were likely contributed by the heavy metal pollution in the Chang-Zhu-Tan city clusters and were comparable to the levels at Mount Lushan [*Li et al.*, 2015]. However, overall, most trace elements at Mount Heng had lower concentrations than those at Mount Dinghu in the Pearl Delta Region [*Yang et al.*, 2009]. Different climate and geographical conditions in northern and southern China and various air pollution around these mountain sites should be responsible for the differences of trace elements concentrations.

The dust storms made large, but different, contributions to individual trace element concentrations. As shown in Table 1, crust-related elements such as Al, Fe, Mn, Cr, Ba, and V increased in coarse and fine aerosols by approximately 3–11 times and 2–13 times, respectively, and the trace elements Zn, Se, Mo, and Ni were elevated approximately onefold to twofold. Pb and Cu showed increased concentrations in coarse aerosols

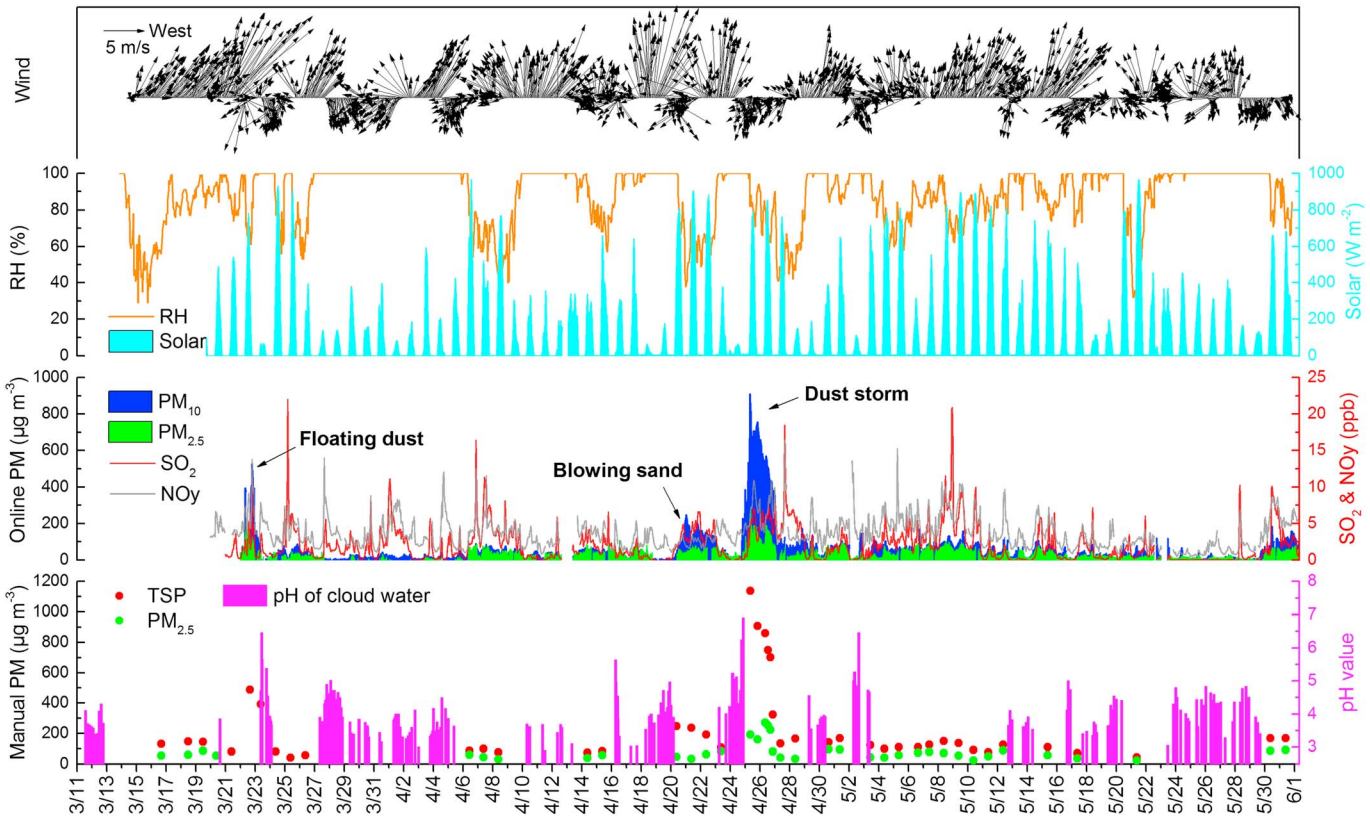

Figure 1. Time series of manual TSP, $PM_{2.5}$ and cloud water samples, continuous PM_{10} and $PM_{2.5}$ aerosols, trace gases SO_2 and NO_y, and meteorological parameters RH and solar radiation at Mount Heng from 11 March to 31 May 2009. The start time (UTC + 8) of the manual sampling is indicated.

Table 1. Concentrations (Mean ± SD, ng m^{-3}) of Trace Elements in $PM_{2.5}$ and TSP Aerosols at Mount Heng During Nondust (ND) and Dust Storm (DS) Periods and Comparison With Other Mountain Sites in China

	Mt. Heng				Mt. Tai[a]		Mt. Lushan[b]	Mt. Dinghu[c]
	$PM_{2.5}$		TSP					
Species	ND	DS	ND	DS	$PM_{2.5}$	TSP	$PM_{2.5}$	$PM_{2.5}$
Fe	510.5 ± 345.4	3672 ± 1470	1577 ± 1347	17980 ± 9379	810	2180	331.6	569.8
Al	208.2 ± 170.6	2833 ± 1267	851.2 ± 769.9	8492 ± 4646	1200	3010	515.1	914.1
Zn	171.7 ± 105.5	315.9 ± 190.1	349.2 ± 218.2	529.7 ± 430.3	400	490	245.3	432.1
Pb	108.6 ± 50.9	102.3 ± 29.8	124.3 ± 56.0	144.2 ± 52.2	15.2	42.2	70.5	216.2
Ba	13.8 ± 5.20	33.5 ± 16.3	186.6 ± 174.0	577.0 ± 430.7			61.9	14.2
Mn	44.6 ± 24.7	137.1 ± 54.9	69.6 ± 37.5	367.2 ± 176.2	39.1	75.3	20.2	33.1
As	21.1 ± 12.4	16.5 ± 10.6	38.4 ± 29.1	36.6 ± 10.9	2.3	5.71	20.9	31.8
Cu	14.6 ± 8.20	12.2 ± 11.0	49.6 ± 45.0	84.3 ± 68.6	24	57	11.7	60.6
Cr	8.85 ± 9.50	30.6 ± 11.9	17.0 ± 13.6	83.1 ± 30.1	22.9	23	9.6	
Se	5.20 ± 2.20	6.26 ± 1.85	6.67 ± 2.71	11.7 ± 2.25			6.5	8.1
Cd	5.55 ± 3.47	3.19 ± 1.14	7.97 ± 5.47	5.02 ± 2.33	1.0	1.3	2.2	7.0
Sb	2.93 ± 2.26	0.88 ± 0.53	10.6 ± 6.47	7.68 ± 4.19				8.4
Ni	2.92 ± 2.06	3.41 ± 1.55	7.03 ± 4.55	30.7 ± 8.80	7.4	7.5		6.5
V	1.78 ± 1.82	4.02 ± 3.15	4.54 ± 2.94	29.4 ± 10.3		5.4		15.4
Mo	0.57 ± 0.34	1.08 ± 0.65	2.26 ± 2.02	3.23 ± 2.50			1.5	1.4

[a]Spring 2006/2007, frequently affected by sand dust in the North China Plain [*Deng et al.*, 2011].
[b]Spring 2012, in the neighboring Jiangxi Province in southern China [*Li et al.*, 2015].
[c]June–December 2006, which suffered severe air pollution in the Pearl River Delta region [*Yang et al.*, 2009].

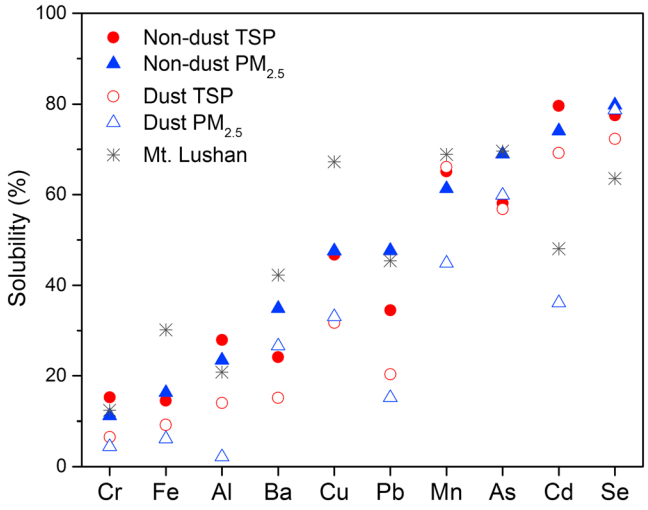

Figure 2. Solubility of trace elements in TSP and $PM_{2.5}$ at Mount Heng (this study) and in $PM_{2.5}$ at Mount Lushan [*Li et al.*, 2015].

and comparable in fine aerosols. Apparently, the dust storms brought abundant crustal elements and the entrainment of air pollution lead to the increase of many anthropogenic elements. As, Cd, and Sb exceptionally decreased both in coarse and fine aerosols, probably due to relatively lower emissions of these anthropogenic elements in the dust storm pathways than other regions in addition to the dilution effect of dust plumes.

Figure 2 shows the trace element solubility in coarse and fine aerosols at Mount Heng. Here the solubility concept was defined as the percentage of the water-soluble concentration of an element to its total fraction, indicating the dissolution capacity of aerosol trace elements. Most elements had similar solubility in coarse and fine aerosols during nondust periods, while As, Pb, and Ba appeared to be more soluble in fine mode than coarse mode, with a solubility discrepancy of ~10%. In addition, trace elements in fine aerosols at Mount Heng showed approximately comparable solubility with those at Mount Lushan [*Li et al.*, 2015], except for more soluble Se and Cd and less soluble Cu and Fe. However, the declined solubility of trace elements in both coarse and fine aerosols during dust periods was clearly observed, indicating the suppressed dissolution of aerosol elements by dust storms, which was largely attributable to the decreased aerosol acidity (see Text S3) from abundant alkaline substances.

3.3. Trace Elements in Cloud Water

3.3.1. Concentrations

Table 2 presents the concentration levels of dissolved trace elements in cloud water at Mount Heng. Zn was found to be the predominant element with a VWM concentration of 224.6 $\mu g\,L^{-1}$, almost the same level as the values at Mount Lushan [*Sun et al.*, 2015] and Mount Tai [*Liu et al.*, 2012]. Higher concentrations of Fe (155.2 $\mu g\,L^{-1}$) than Al (99.7 $\mu g\,L^{-1}$) were observed, exactly opposite to the results at Mount Lushan and Mount Tai where higher concentrations of Al were measured instead of Fe, but matching the concentration order of Fe and Al in aerosols at Mount Heng. Toxic Pb (100.5 $\mu g\,L^{-1}$) in cloud water was determined to be twice as high as the values at Mount Lushan and Mount Tai, and other trace elements such as As, Cu, and Cd also showed slightly higher concentration levels. Compared to Mount Schmücke [*Fomba et al.*, 2015] and Mount Elden [*Hutchings et al.*, 2008], most of the trace elements, especially Pb, As, Ni, and Se, at Mount Heng exhibited markedly higher concentrations, suggesting the serious toxic heavy metal pollution

Table 2. Volume-Weighted Mean (VWM) Concentrations ($\mu g\,L^{-1}$) of Trace Elements in Cloud Water at Mount Heng and Other Mountain Sites

Sites	pH	Zn	Fe	Pb	Al	Mn	As	Ba	Cu	Ni	Se	Cd	Sb	V	Cr	Mo
Mt. Heng																
VWM	3.80	224.6	155.2	100.5	99.7	34.0	19.9	12.7	11.7	7.15	5.66	4.05	2.56	2.26	1.61	0.95
Max	6.91	3527	876	1421	1872	694	213	138	424	81.7	58.3	84	31.8	29.2	14.3	6.96
Min	2.91	0.11	12.3	0.01	0.01	0.49	0.01	0.01	0.01	0.46	0.56	0.18	0.01	0.16	0.01	0.4
Mt. Lushan[a]	3.79	179.2	25.75	54.4	111.9	16.4	20.4	23.9	7.97	4.4	7.4	1.66	0.77	5.9	8.37	0.8
Mt. Tai[b]	3.95	249.1	105.8	46.2	157.3	42.8	13.7		9.2	9.3		3.08			0.93	
Mt. Schmücke[c]	4.30			1.4		5.59	0.63				1.38			0.71	5.54	
Mt. Elden[d]	6.34		5.6	0.4	16.6	34	0.8	15.2	25	5.7	2			3.2	1.7	

[a]August–September 2011 and March–May 2012 in southern China [*Sun et al.*, 2015].
[b]March 2007 to November 2008 in the North China Plain [*Liu et al.*, 2012].
[c]September and October 2011 in Germany [*Fomba et al.*, 2015].
[d]Median concentrations, summers of 2005–2007 in southwestern America [*Hutchings et al.*, 2008].

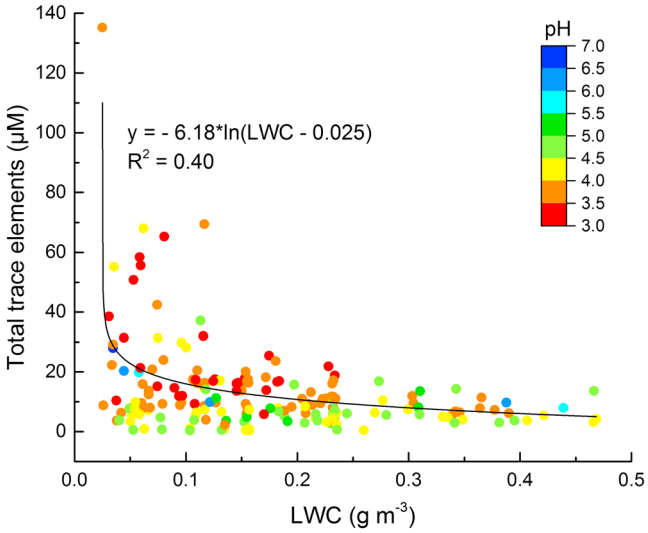

Figure 3. Relationship between total concentration of the dissolved trace elements (including Al, V, Cr, Mn, Fe, Ni, Cu, Zn, As, Se, Mo, Cd, Sb, Ba, and Pb) and LWC for 192 cloud water samples at Mount Heng.

of cloud water. A wide range of concentration variations (approximately 1–5 orders of magnitudes) of cloud water trace elements is also shown in Table 2.

3.3.2. Dependencies on LWC and pH

Many factors such as particle sources, acidity of cloud drops, and aging processes [*Deguillaume et al*., 2005] can influence the dissolution of trace elements in cloud water. In this study, the LWC and pH of cloud water were found to have important effects on dissolved trace elements.

LWC has been acknowledged as an important factor that controls solute concentrations in cloud water, with complicated inverse relationships such as power laws [*Elbert et al*., 2000; *Möller et al*., 1996] or exponential functions [*Aleksic and Dukett*, 2010]. Similar inverse relationships between dissolved trace elements and LWC are also visible at Mount Heng, as shown in Figure 3 (and Figure S6). The difference is that the inverse relationships in this study could only be well fitted by logarithmic functions. Additionally, the fitted curves in this study were fully empirical and may have been regionally limited because of various meteorological and environmental conditions compared to other observation locations.

However, no matter what the fitted curves were, the trace element concentrations sharply decreased as the LWC increased to approximately 0.1 g m^{-3} and then slowly declined with increasing LWC. Small LWC values ($\leq$0.1 g m^{-3}) usually occurred at the beginning or end of a cloud event and during interruptions in clouds by external air masses with longer sampling duration (Figure S7), when intense aerosol-cloud interactions occurred. Therefore, the higher concentrations of trace elements in cloud water at lower LWC ($\leq$0.1 g m^{-3}) were likely caused by greater contributions from ambient aerosol particles from nucleation scavenging and the faster evaporation of smaller cloud drops because of increased CCN. In contrast, larger LWC values ($>$0.1 g m^{-3}) generally appeared during the middle of cloud events, which were characterized by smaller variability and shorter sampling duration (Figure S7). Thus, the slowly decreasing tendency of trace elements with increasing LWC from 0.1 to 0.47 g m^{-3} (Figure 3) could be considered a result of dilution effect in the context of lower entrainment of external air masses. Figure 3 shows notable deviation of scatter points from fitted curve, in addition to the important role of LWC in controlling trace elements concentrations in cloud water. Cloud water samples above the fitted curve with LWC $<$ 0.2 g m^{-3} often exhibited very low pH values ($<$4.0), while samples below the fitted curve across the entire LWC range were mainly characterized by moderate pH values (4.0 to 5.0). The cloud water acidity appeared to have an important influence on the LWC dependency of the trace element concentrations.

Figure 4 displays the concentration distributions of individual trace elements as a function of the cloud water pH values, with five groups divided in terms of the LWC at interval of 0.1 g m^{-3}. Clearly, the trace element concentrations were highly pH dependent: extremely high concentrations were mainly located under a

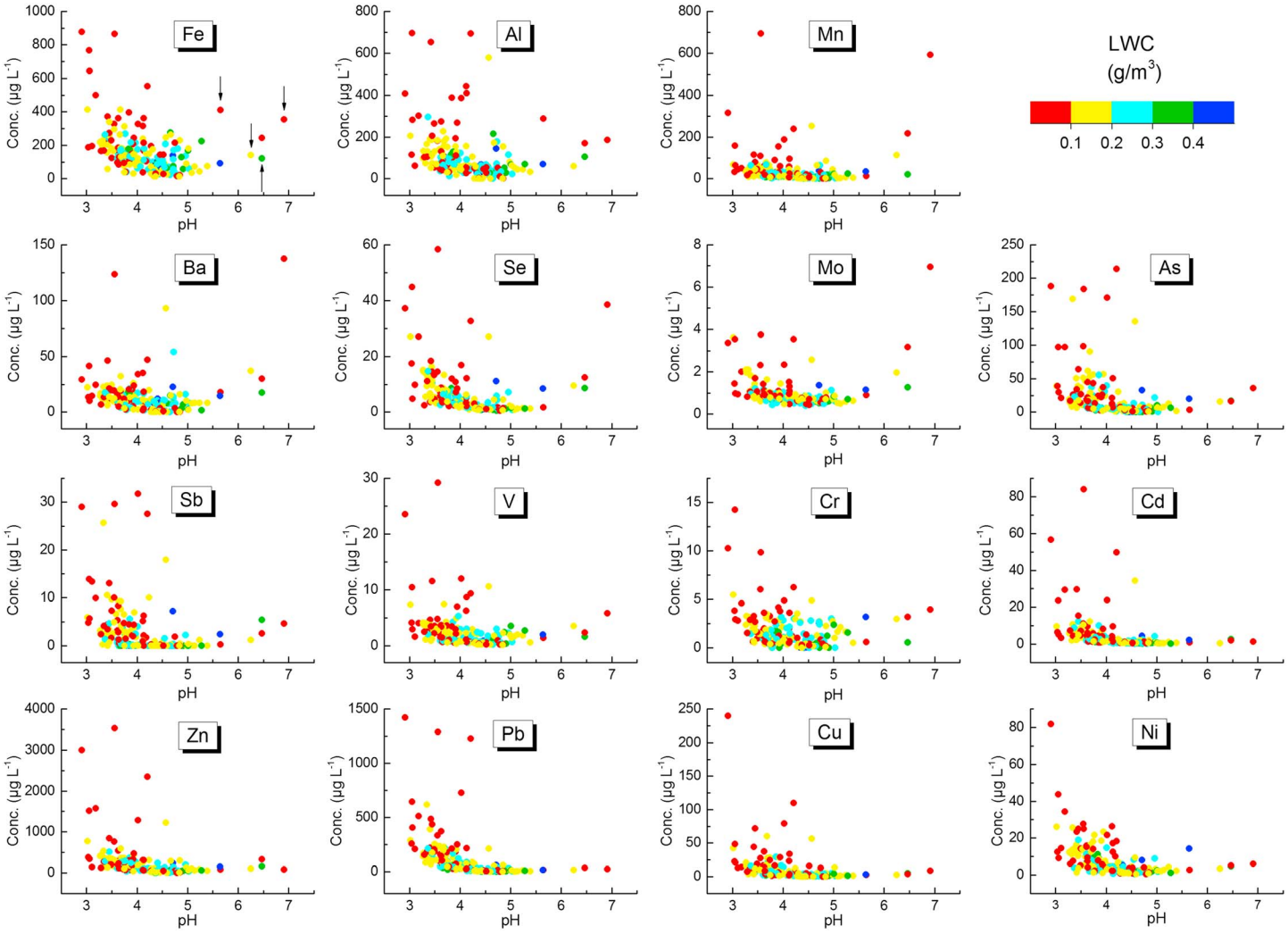

Figure 4. Scatterplots of dissolved trace elements concentrations versus pH values at Mount Heng. Four dust-affected cloud water samples are indicated by arrows.

low pH regime (<4.0), while rapid decreases in concentration were observed with increases in pH from 2.9 to approximately 5.0. Afterward, two different trends in the concentration variations of trace elements were observed: when the pH was higher than 5.0, crustal elements such as Fe, Al, Mn, Ba, and Se presented evidently elevated concentrations, while anthropogenic elements including Zn, Pb, Cu, Ni, and Cd remained nearly constant. Additionally, each LWC group showed an approximately similar distribution tendency for individual trace element, especially for groups with higher LWC ($>0.1\,g\,m^{-3}$). The larger variability of trace elements in samples with lower LWC ($<0.1\,g\,m^{-3}$, red dots in Figure 4) was mainly induced by ACIs as mentioned above, but these samples had comparable concentration distributions. We cautiously inferred that the pH dependency of the element concentrations was barely influenced by the LWC.

The declining trend of metal solubility in rainwater and aerosols with increasing pH was reviewed by *Deguillaume et al.* [2005], and the pH-edge values at which the correlation trend between the metal solubility and pH sharply changed are distinguished. In our field cloud water, a pH of ~5.0 was likely a threshold below which significantly higher element concentrations were observed. Typically, lower pH accelerates the release of trace elements from solid phases by the intense competitive adsorption of H^+ for ligands at acidic pH [*Stumm and Morgan*, 1996]. Thus, the remarkably high concentrations under a low pH regime with low LWC should have resulted from promoted dissolution and contributions from ACIs. However, little is known regarding why crustal elements such as Fe, Al, Mn, and Ba notably increased again above the pH threshold, especially for pH > 5.6. The elevated crustal elements in 4 of the 14 cloud

water samples under a high pH regime (indicated by arrows in Figure 4) were affected by dust storms according to our sampling records. However, no matter if the cloud water samples at pH > 5.0 were affected by dust, the crustal elements exhibited increased concentrations to varying degrees. In fact, the pH-dependent distribution pattern for trace elements in this study was not unique. In our previous work at Mount Tai [*Liu et al*., 2012], where the cloud water pH ranged from 2.56 to 7.64, we similarly found a minimum concentration at a pH of 5.0–6.0 and increasing trends above pH ~6.0 for crustal elements (Figure S8). Further dissolution of dust aerosol Fe at pH above 7.1 was also observed during simulated cloud processing by *Mackie* [2005], which was thought to have been caused by the formation of soluble ferrates. In section 3.3.3, the increase in soluble Fe(III)-hydroxyl complexes by chemical speciation calculation is likely to be a significant reason for the elevated iron under a high pH regime. The pH threshold values in this study were not identical with those in cloud water at Mount Tai and the simulation by *Mackie* [2005] and seemed to be region dependent, because many situations, e.g., types and content of (in)organic ligands and heterogeneous reactions in field cloud water, were varied.

3.3.3. Chemical Speciation

The chemical speciation distribution of dissolved trace elements in cloud water is summarized in Table S3. Generally, 96.3% of the Fe(II), 94.2% of the Zn(II), 88.0% of the Pb(II), and 80.7% of the Cu(II) were present in divalent free ions; 71.7% and 27.5% of the Fe(III) were present in the form of Fe(III)-oxalates and Fe(III)-hydroxyls, respectively; and 71.5% and 19.7% of the Al(III) were complexed by fluoride and oxalate ions, respectively. Oxalate was an important organic ligand, which contributed 0.7–71.7% of the metal complexation, while sulfate only provided 0.2–5.2%, although this compound was the most abundant species in cloud water.

The cloud water acidity significantly influenced the distribution of trace metal speciation, as shown in Figure 5. Fe(II), Zn(II), and Pb(II) had an approximately parallel speciation distribution pattern. Their dominant free ions stayed at very large percentages from pH 4.2 to 5.3 and then decreased. On the contrary, sulfuric complexes stepwise decreased before a pH of 4.2 and began to return to their previous levels at pH higher than 5.3. A similar speciation distribution pattern for Cu(II) was obtained, except that the free Cu^{2+} showed no maximum but rather declined with increasing pH.

However, dissolved Fe(III) showed quite distinctive speciation distribution patterns. The dominant Fe(III)-oxalato complexes gradually vanished from 91% and the Fe(III)-hydroxyl species significantly increased from 5% to 98% as the pH values increased. Meanwhile, minor species such as free ferric ion and sulfato and fluoro complexes were only found at pH below 4.0. Figure S9a displays the variation curves of specific Fe(III) species that were mainly complexed by oxalate and hydroxyls. Clearly, $[Fe(Oxalate)]^+$ and $[Fe(Oxalate)_2]^-$ were the two main Fe(III) species at pH below 4.4, comprising 55–94% of dissolved Fe(III). The dominated Fe(III)-oxalate complex could have been an important contributor to the high concentration of dissolved Fe in cloud water under a low pH regime (Figure 4) because oxalate can improve dust iron solubility as efficiently as acid processes [*Paris et al*., 2011], probably via the formation of soluble oxalic complexes and/or the concomitant photoreduction of Fe(III)-oxalato complexes to more soluble Fe(II) [*Chen and Grassian*, 2013; *Paris and Desboeufs*, 2013]. As the cloud water acidity decreased, oxalic complexation declined and $[Fe(OH)_2]^+$ rapidly became the most predominant Fe(III) speciation. $[Fe(OH)]^{2+}$ only slightly increased until its maximum at a pH of 4.5. $Fe(OH)_3(aq)$ species were observed in circumneutral cloud water at pH > 5.6, and soluble ferrates $[Fe(OH)_4]^-$ even formed in the sample with the highest pH (6.91), although these compounds comprised less than 0.3% of the total Fe(III). This result adequately indicated the dissolution of precipitated iron (e.g., goethite, α-FeOOH) in neutral cloud drops through form transformation because the solubility of amphoteric metal hydroxide theoretically increases at high pH from the strong competition of OH^- with other ligands [*Stumm and Morgan*, 1996].

The variations in the dissolved Al(III) complexes were more complicated. Briefly, the major fluoro complexes gradually decreased, while oxalic and hydroxy-oxalic complexes increased quickly with rising pH. The speciation curves in Figure S9b further distinguished $[AlF_2]^+$ and $[Al(OH)_2\text{-Oxalate}]^-$ as the primary complexing forms under a low pH regime (pH < 4.0) and very high pH regime (pH > 6.0), respectively. $[AlF_2]^+$ and $[AlF]^{2+}$ decreased across the entire pH range, while $[Al(Oxalate)]^+$ and $[Al(Oxalate)_2]^-$ rose to their maximum at a pH of 4.8 and decreased afterward. Al(OH)-Oxalate, which peaked at a pH of 5.5, presented a similar but lagging curve compared to the oxalato complexes, and $[Al(OH)_2\text{-Oxalate}]^-$ accordingly boomed from 3% to

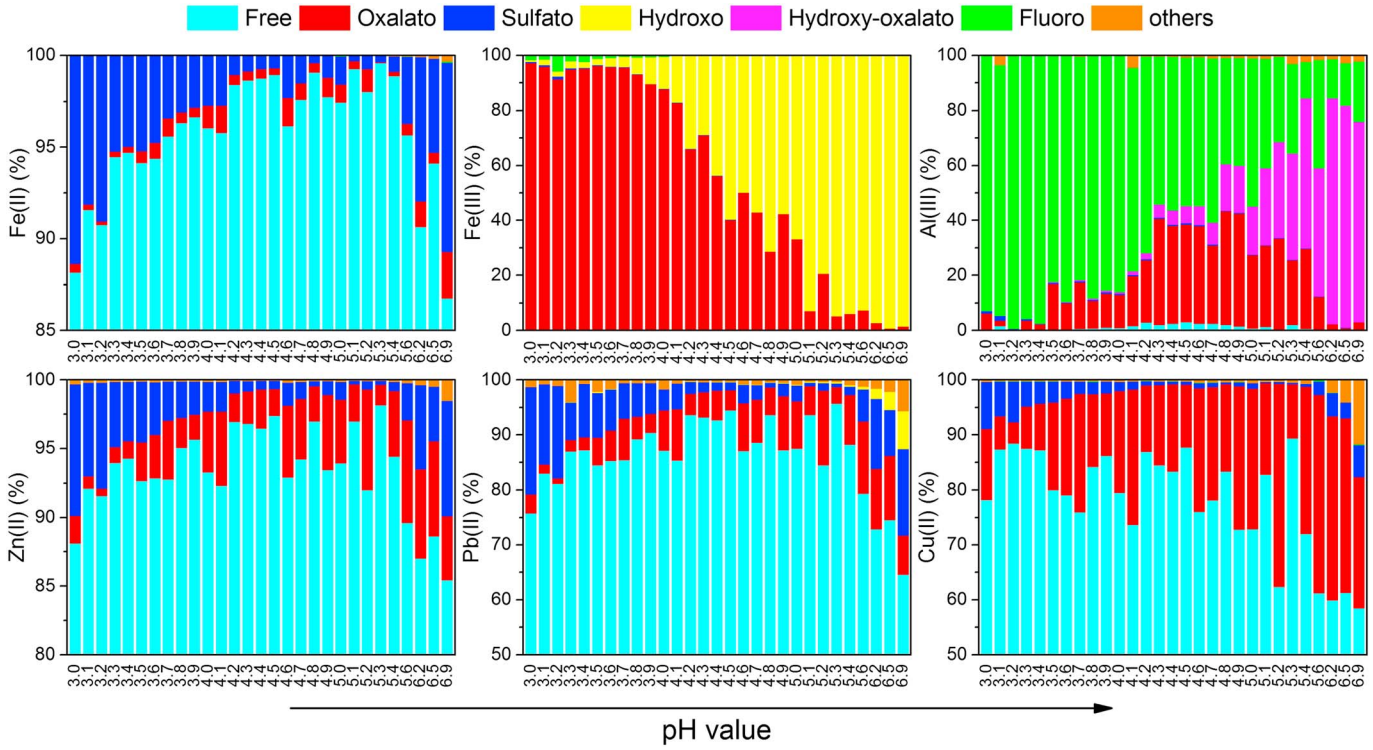

Figure 5. Distribution patterns of the calculated equilibrium complexation of dissolved trace elements as a function of cloud water pH at Mount Heng. "Free" represents uncomplexed metals. Complexes such as "oxalato Fe(III)" comprise $[Fe(Oxalate)_3]^{3-}$, $[Fe(Oxalate)_2]^{-}$, and $[Fe(Oxalate)]^{+}$. Other categories are defined in the same manner, except the "others" group, which contains metals that were complexed by organic and inorganic ligands such as formate, acetate, lactate, nitrate, and chloride.

70% at a pH regime of 5.0–6.9. The complexing ligands of Al(III) were stepwise substituted by OH^{-} as the pH increased, forming anionic hydroxide-ligand complexes. In conclusion, the chemical speciation of dissolved trace elements was highly pH dependent, and the formation of soluble hydroxo complexes could have been vital for the dissolution of iron and aluminum under a high pH regime.

3.4. ACI Effects on Trace Element Evolution

3.4.1. Influence of Dust Aerosols on Cloud Water Trace Elements

Figure 6 displays the temporal variations in the concentration and speciation of dissolved Fe(III), Al(III), and Cu (II) in selected cloud events to investigate the influence of dust aerosols on cloud water trace elements. When comparing these concentrations, the equivalent air concentrations, which are defined as the multiplication of the solute concentrations with the LWC, were employed to remove the interference of dilution variability during cloud processes.

A significant increase in cloud water pH values was observed at the end of the dust storm on 23 March (Figure 6a) and the arrival of the dust storm on 24 April (Figure 6b) because of neutralization by abundant alkaline substances in dust aerosols. The exceptional pH of 4.7 from the first sample in Figure 6a can be ascribed to much more abundant sulfate (37.4 mg L^{-1}) and nitrate (26.2 mg L^{-1}), which formed from their enhanced precursors SO_2 and NO_y (Figure S3a). The notable elevation in the equivalent air concentrations of Fe, Al, and Cu in dust-affected cloud water demonstrated large contributions of trace elements from aerosol particles to cloud condensation. Changes in the speciation distribution patterns of trace elements in cloud water were also observed. However, we are not sure whether these changes originated from the direct dissolution of the preserved speciation in the precloud particulate phase or from the recombination of dissolved metal ions with ligands in cloud drops. If we assume that the contributions from air masses to cloud events in Figure 6a over the first 3 h were constant, this speciation should have remained approximately identical if these materials were directly derived from the preserved speciation in aerosol particles. However, the opposite was true: the speciation varied greatly with different pH values. Moreover, the chemical speciation of

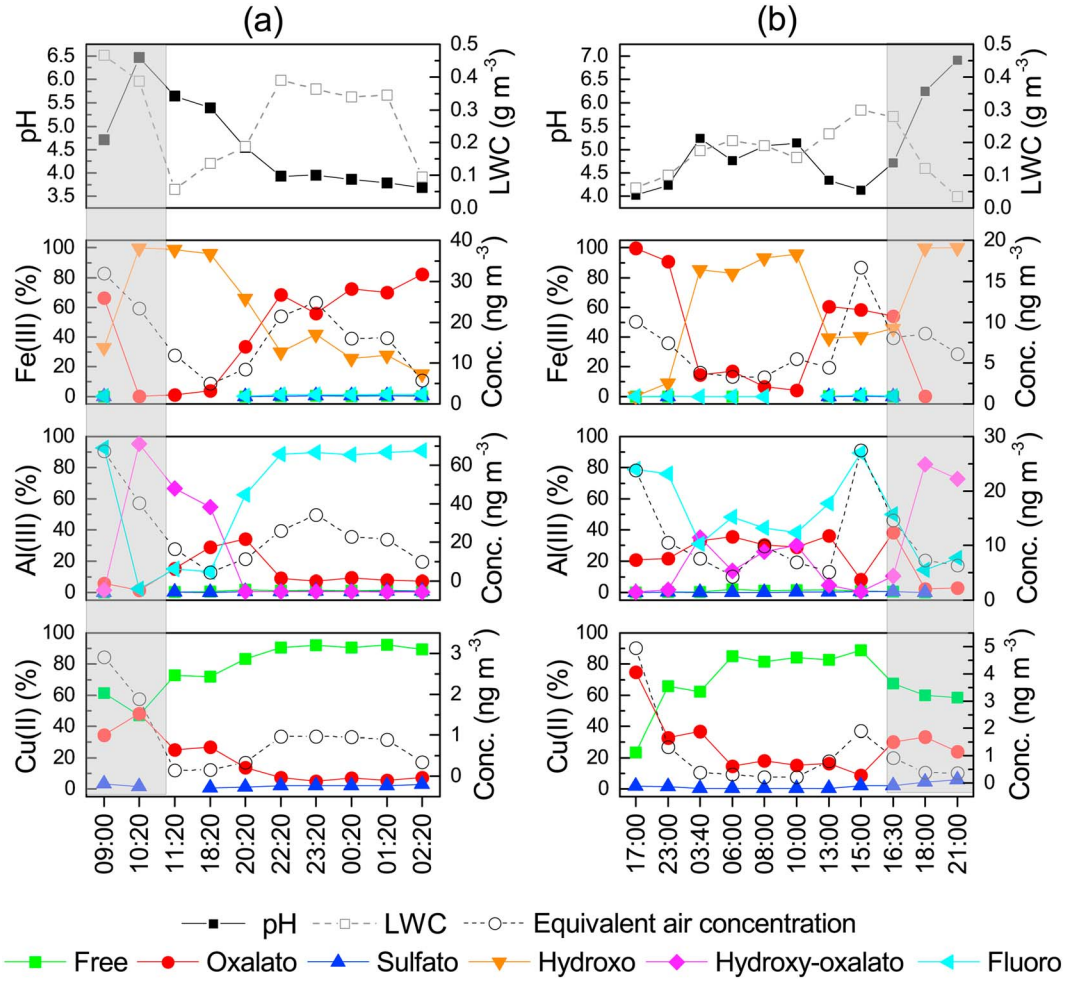

Figure 6. Temporal variation in cloud water pH, LWC, equivalent air concentration, and chemical speciation of dissolved Fe (III), Al(III), and Cu(II) during cloud events on (a) 23–24 March after dust storms and (b) 23–24 April before dust storms. The shaded areas indicate dust storm periods. The Fe(III) concentrations are half the total dissolved Fe.

dissolved Fe(II), Fe(III), and Cu(II) in this study was quite different from their complexing forms in aerosol liquid phases as calculated by *Scheinhardt et al.* [2013]. We believe that the chemical speciation of these trace elements in cloud water was modified from the preserved species in dust aerosols because of the sharp changes in solution acidity and ligands availability.

3.4.2. In-Cloud Scavenging Effects

Figure 7 shows an evident decrease in the $PM_{2.5}$ concentration during the two selected cloud events on 12 and 18 May 2009, which demonstrates the significant effects of in-cloud scavenging on aerosol removal. More importantly, aerosol particles quickly and heavily declined within only 2–3 h, after which their concentrations remained at a relatively lower and constant level. That is, fine aerosols were mostly removed by cloud processing during the initial few hours, reaching maximum scavenging ratios of approximately 0.80 and 0.68 for the two cloud events. Trace elements in cloud drops are only derived from the incorporation and dissolution of aerosol particles, so the first cloud water samples whose sampling periods (2–3 h, indicated by the light blue shadows in Figure 7) approximately coincided with the maximum scavenging of aerosols were believed to be appropriate to measure the in-cloud scavenging of aerosol trace elements. Thus, each trace element showed different scavenging ratios, ranging from 0.11 for Cr (0.15 for Cr) to 0.56 for Pb (0.57 for As) for the cloud process on 12 May (18 May) 2009. The results in this study were acceptable compared to the various scavenging ratios for different chemical species (e.g., water-soluble ions and organics) by different types of clouds, as summarized by *Ervens* [2015], because numerous factors such as the different solubility

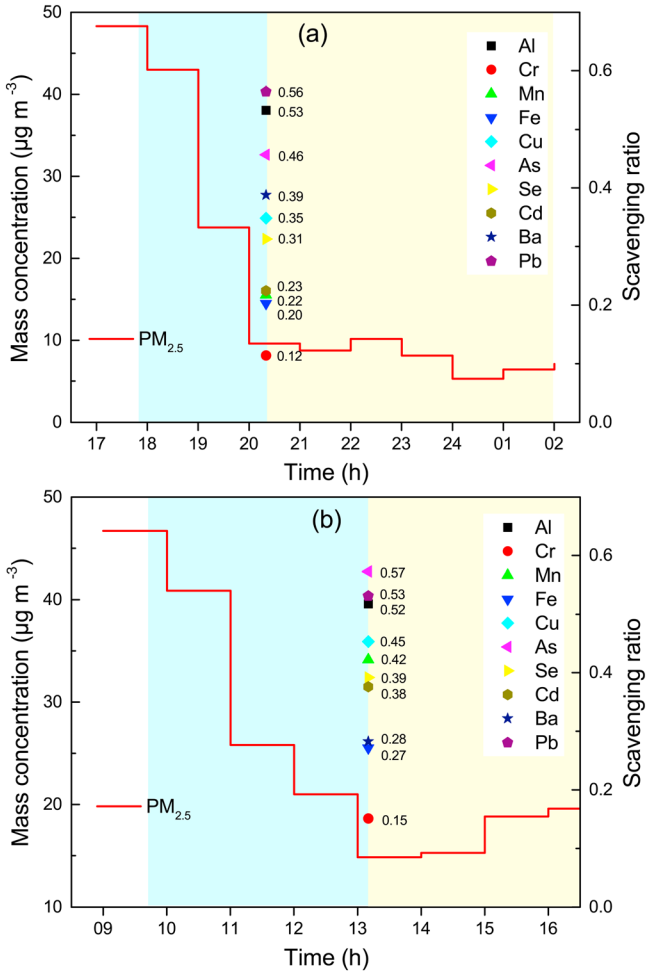

Figure 7. $PM_{2.5}$ mass concentration variation (red line) and in-cloud scavenging ratios for trace elements (colored symbols) during cloud events on (a) 12 May 2009 and (b) 18 May 2009. The light blue and yellow shadows indicate the periods of the first and subsequent cloud water samples, respectively. See the text for details on the calculations.

and size distributions of chemical species in particles and cloud drops [*Fomba et al.*, 2015; *Hoag et al.*, 1999; *Lin et al.*, 2015] may significantly influence their in-cloud scavenging. In the case of less aerosol particle contributions (scavenging) to cloud process on 18 May, most of the trace elements still had comparable or slightly higher scavenging ratios than on 12 May. The promoted dissolution of trace elements by the lower cloud water pH on 18 May (pH = 3.37, LWC = 0.23 g m^{-3}) than on 12 May (pH = 3.77, LWC = 0.18 g m^{-3}) might have been to blame according to their pH-dependent concentrations in Figure 4. The in-cloud scavenging effects on all the trace elements should have been underestimated to different extent because their undissolved portions that remained in cloud residues were not included in the calculation, which was reflected by the higher scavenging ratios for fine particles than trace elements.

3.4.3. Modification of Aerosol Trace Element Solubility by Cloud Processing

During the dust ACIs event on 23–24 March 2009, an in-cloud TSP sample was synchronously collected from the beginning of the cloud event from 9:30 to 11:20 A.M. (Figure S3a). Figure 8 demonstrates an obvious increase in solubility for each trace element in both in-cloud aerosols (4% for Se to 28% for As) and postcloud aerosols (4% for Fe to 33% for As) by cloud processing. The lower solubility of trace elements in the precloud aerosols was likely related to their crystal structure in mineral dusts, even if the abundant sulfate (45.5 μg m^{-3}) and nitrate (9.9 μg m^{-3}) in the dust aerosols could not efficiently improve the trace element solubility. Given that the calcium was primarily from natural dusts, we used the equivalent mole ratio of secondary SO_4^{2-}, NO_3^-, and NH_4^+ to Ca^{2+} to roughly estimate their net variation. Apparently, higher [SO_4^{2-}]/[Ca^{2+}] and [NH_4^+]/[Ca^{2+}]

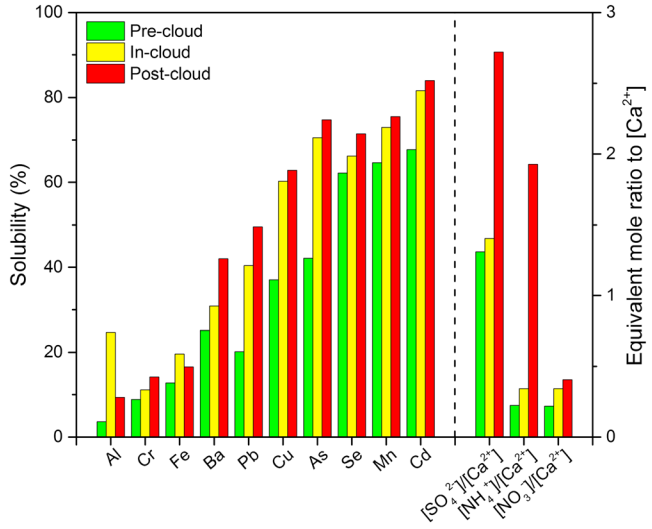

Figure 8. Trace element solubility (left of the dashed line) and equivalent mole ratio of secondary sulfate, ammonia, and nitrate to calcium (right of the dashed line) in precloud, in-cloud, and postcloud TSP aerosols during the dust ACIs on 23–24 March 2009.

ratios were observed in cloud-processed aerosols, which suggested that more in-cloud formation of secondary ions, particularly SO_4^{2-}, should always occur against the cloud scavenging of dust aerosols. The heterogeneous oxidation of SO_2 that is catalyzed by transition metal ions such as Fe^{3+} and Cu^{2+} proves large contributions to sulfate production in cloud aqueous phases [*Harris et al.*, 2013], which could further increase the acidity of cloud drops and thus promote the dissolution of trace elements in particulate phases. Solubilization is generally irreversible, so dissolved trace elements in cloud drops would remain associated with cloud-processed aerosols after cloud evaporation and lead to the enhancement of aerosol trace element solubility.

Additionally, the solubility of trace elements in in-cloud aerosols showed significantly large increases, which were 34–90% (for Ba to Cu), 181% (for Fe), and 365% (for Al) of their solubility increases in postcloud aerosols, indicating that the first 2 h of cloud processing (the sampling duration of the in-cloud TSP sample) could have substantially promoted the aerosol elements' dissolution. The modification of metal particle morphology or complexing states by ACIs was supposed to have greatly contributed to the solubility increases because *Shi et al.* [2009] proved that the increased Fe solubility in Saharan dusts during simulated cloud processes was caused by the formation of amorphous Fe nanoparticles.

4. Conclusions

This study investigated the effects of dust storms and aerosol-cloud interactions on chemical evolution of trace elements in aerosols and cloud in the planetary boundary layer. Generally, dust storms provided large contributions to the crust-related elements in both coarse and fine aerosols, except for the lower amounts of fine aerosol Pb, Cu, As, Cd, and Sb. In contrast, most of the trace elements showed evidently inhibited solubility because the aerosols became more alkaline.

Trace elements in the cloud water had similar concentrations to those in aerosols; in particular, high concentrations of toxic Pb, Cu, and Cd were observed. The LWC had complicated dilution effects on the concentrations of dissolved trace elements, as the logarithmic inverse relationships were found. Intense aerosol-cloud interactions likely lead to the very high concentrations of trace elements which had low LWC ($\leq$0.1 g m^{-3}) and low pH values ($<$4.0). Importantly, the dissolution of trace elements was highly pH dependent and the lowest concentrations were observed at a threshold of pH ~5.0. The pH threshold values in this study should be region dependent and the chemical speciation of trace elements which were also pH dependent might be a determinant. The elevated trace elements under a low pH regime were mainly released from the solid phases by the strong protonation of acid cloud drops, while the increased crustal elements under a high pH regime might have been induced by the formation of soluble hydroxo metal complexes in neutral cloud water as indicated by the calculation result.

Significant effects of ACIs on trace elements were demonstrated in the field observation. ACIs induced the evident changes in the chemical speciation of trace elements in the first several cloud water samples by altering the droplets acidity. At the same time, trace elements were primarily removed by in-cloud nucleation scavenging within the first 2–3 h on the basis of the dramatic decline of $PM_{2.5}$ mass. The higher scavenging ratios for aerosol particles indicated that the scavenging of trace elements was likely underestimated because

portions that remained in cloud residues were not considered here. In future studies, the actual concentrations of undissolved trace elements should be determined to obtain more accurate scavenging ratios. ACIs also created 4–33% of the increases in the aerosol trace elements' solubility, making appreciable contributions to the mobility and reactivity of transition metals (e.g., Fe, Cu, and Mn), and the bioavailability and toxicity of heavy metals (e.g., Pb, As, and Cd) in aerosol particles. The notably increased solubility that was observed in in-cloud aerosols indicated that enhancement of aerosol trace elements solubility could be considerably achieved during the first 2 h of cloud processing.

This study highlights the effects of aerosol-cloud interactions on the speciation, solubilization, and scavenging of atmospheric trace elements within the initial few hours. As small convective clouds and deep clouds are estimated to have lifetimes of 0.5–1 h and 2–3 h, respectively [*Warneck*, 1999], our findings imply that the first several cloud cycles (conservatively ~1–3 cycles on average) could be crucially important to the chemical evolution of trace elements. Knowledge of the dynamic chemical changes of trace elements, in particular transition metals, during aerosol-cloud interaction events is vital to understand their impacts on atmospheric chemistry.

Acknowledgments

The authors wish to appreciate Penghui Li, Minghu Sun, Jia Guo, and Yuhua Li from Shandong University for the help of field experiments. Thanks also to Taixing Yue and Yanfang Zhao for their assistance in trace elements measurements. We are grateful to all the staff of Mount Heng Meteorological Station for providing the field observation platform and meteorological data. This work was funded by the National Key Research and Development Program of China (2016YFE0112200) and the National Natural Science Foundation of China (41475115). There are no conflicts of interest in the article. The supporting data can be found in Table S1 and also available on request to Yan Wang (wy@sdu.edu.cn).

References

Aleksic, N., and J. E. Dukett (2010), Probabilistic relationship between liquid water content and ion concentrations in cloud water, *Atmos. Res.*, *98*(2–4), 400–405, doi:10.1016/j.atmosres.2010.08.003.

Chen, H., and V. H. Grassian (2013), Iron dissolution of dust source materials during simulated acidic processing: The effect of sulfuric, acetic, and oxalic acids, *Environ. Sci. Technol.*, *47*(18), 10,312–10,321, doi:10.1021/es401285s.

Cini, R., F. Prodi, G. Santachiara, F. Porcu, S. Bellandi, A. Stortini, C. Oppo, R. Udisti, and F. Pantani (2002), Chemical characterization of cloud episodes at a ridge site in Tuscan Appennines, Italy, *Atmos. Res.*, *61*(4), 311–334.

Deguillaume, L., M. Leriche, K. Desboeufs, G. Mailhot, C. George, and N. Chaumerliac (2005), Transition metals in atmospheric liquid phases: Sources, reactivity, and sensitive parameters, *Chem. Rev.*, *105*(9), 3388–3431, doi:10.1021/cr040649c.

Deng, C., et al. (2011), Chemical characterization of aerosols at the summit of Mountain Tai in Central East China, *Atmos. Chem. Phys.*, *11*(14), 7319–7332, doi:10.5194/acp-11-7319-2011.

Eck, T. F., et al. (2012), Fog- and cloud-induced aerosol modification observed by the Aerosol Robotic Network (AERONET), *J. Geophys. Res.*, *117*, D07206, doi:10.1029/2011JD016839.

Elbert, W., M. R. Hoffmann, M. Krämer, G. Schmitt, and M. O. Andreae (2000), Control of solute concentrations in cloud and fog water by liquid water content, *Atmos. Environ.*, *34*(7), 1109–1122, doi:10.1016/S1352-2310(99)00351-9.

Ervens, B. (2015), Modeling the processing of aerosol and trace gases in clouds and fogs, *Chem. Rev.*, *115*(10), 4157–4198, doi:10.1021/cr5005887.

Fomba, K. W., K. Müller, D. van Pinxteren, and H. Herrmann (2013), Aerosol size-resolved trace metal composition in remote northern tropical Atlantic marine environment: Case study Cape Verde islands, *Atmos. Chem. Phys.*, *13*(9), 4801–4814, doi:10.5194/acp-13-4801-2013.

Fomba, K. W., D. van Pinxteren, K. Müller, Y. Iinuma, T. Lee, J. L. Collett, and H. Herrmann (2015), Trace metal characterization of aerosol particles and cloud water during HCCT 2010, *Atmos. Chem. Phys.*, *15*(15), 8751–8765, doi:10.5194/acp-15-8751-2015.

Ghauri, B. M., M. I. Mirza, R. Richter, V. A. Dutkiewicz, A. Rusheed, A. R. Khan, and L. Husain (2001), Composition of aerosols and cloud water at a remote mountain site (2.8 kms) in Pakistan, *Chemosphere: Global Change Sci.*, *3*(1), 51–63.

Graedel, T. E., C. J. Weschler, and M. L. Mandich (1985), Influence of transition metal complexes on atmospheric droplet acidity, *Nature*, *317*(6034), 240–242.

Harris, E., et al. (2013), Enhanced role of transition metal ion catalysis during in-cloud oxidation of SO_2, *Science*, *340*(6133), 727–730, doi:10.1126/science.1230911.

Herrmann, H., T. Schaefer, A. Tilgner, S. A. Styler, C. Weller, M. Teich, and T. Otto (2015), Tropospheric aqueous-phase chemistry: Kinetics, mechanisms, and its coupling to a changing gas phase, *Chem. Rev.*, *115*(10), 4259–4334, doi:10.1021/cr500447k.

Hoag, K. J., J. J. L. Collett, and S. N. Pandis (1999), The influence of drop size-dependent fog chemistry on aerosol processing by San Joaquin Valley fogs, *Atmos. Environ.*, *33*(29), 4817–4832, doi:10.1016/S1352-2310(99)00268-X.

Hutchings, J. W., M. S. Robinson, H. McIlwraith, J. Triplett Kingston, and P. Herckes (2008), The chemistry of intercepted clouds in Northern Arizona during the North American monsoon season, *Water Air Soil Pollut.*, *199*(1–4), 191–202, doi:10.1007/s11270-008-9871-0.

Junge, C. E. (1963), *Air Chemistry and Radioactivity*, Academic Press, New York.

Kaufman, Y. J., and I. Koren (2006), Smoke and pollution aerosol effect on cloud cover, *Science*, *313*(5787), 655–658.

Lee, S. H. (2004), New particle formation observed in the tropical/subtropical cirrus clouds, *J. Geophys. Res.*, *109*, D20209, doi:10.1029/2004JD005033.

Li, T., Y. Wang, W. J. Li, J. M. Chen, T. Wang, and W. X. Wang (2015), Concentrations and solubility of trace elements in fine particles at a mountain site, southern China: Regional sources and cloud processing, *Atmos. Chem. Phys.*, *15*(15), 8987–9002, doi:10.5194/acp-15-8987-2015.

Lihavainen, H., V. M. Kerminen, and L. A. Remer (2010), Aerosol-cloud interaction determined by both in situ and satellite data over a northern high-latitude site, *Atmos. Chem. Phys.*, *10*(22), 10,987–10,995, doi:10.5194/acp-10-10987-2010.

Lin, Y. C., C. J. Tsai, Y. C. Wu, R. Zhang, K. H. Chi, Y. T. Huang, S. H. Lin, and S. C. Hsu (2015), Characteristics of trace metals in traffic-derived particles in Hsuehshan Tunnel, Taiwan: Size distribution, potential source, and fingerprinting metal ratio, *Atmos. Chem. Phys.*, *15*(8), 4117–4130, doi:10.5194/acp-15-4117-2015.

Liu, X. H., K. M. Wai, Y. Wang, J. Zhou, P. H. Li, J. Guo, P. J. Xu, and W. X. Wang (2012), Evaluation of trace elements contamination in cloud/fog water at an elevated mountain site in Northern China, *Chemosphere*, *88*(5), 531–541, doi:10.1016/j.chemosphere.2012.02.015.

Mackie, D. S. (2005), Simulating the cloud processing of iron in Australian dust: pH and dust concentration, *Geophys.Res. Lett.*, *32*, L06809, doi:10.1029/2004GL022122.

Malcolm, E. G., G. J. Keeler, S. T. Lawson, and T. D. Sherbatskoy (2003), Mercury and trace elements in cloud water and precipitation collected on Mt. Mansfield, Vermont, *J. Environ. Monitor.*, *5*(4), 584–590, doi:10.1039/b210124f.

Mao, J., S. Fan, D. J. Jacob, and K. R. Travis (2013), Radical loss in the atmosphere from Cu-Fe redox coupling in aerosols, *Atmos. Chem. Phys.*, *13*(2), 509–519, doi:10.5194/acp-13-509-2013.

Möller, D., K. Acker, and W. Wieprecht (1996), A relationship between liquid water content and chemical composition in clouds, *Atmos. Res.*, *41*(3–4), 321–335.

Nie, W., et al. (2012), Asian dust storm observed at a rural mountain site in southern China: Chemical evolution and heterogeneous photochemistry, *Atmos. Chem. Phys.*, *12*(24), 11,985–11,995, doi:10.5194/acp-12-11985-2012.

Parazols, M., A. Marinoni, P. Amato, O. Abida, P. Laj, and G. Mailhot (2006), Speciation and role of iron in cloud droplets at the puy de Dôme station, *J. Atmos. Chem.*, *54*(3), 267–281, doi:10.1007/s10874-006-9026-x.

Paris, R., and K. V. Desboeufs (2013), Effect of atmospheric organic complexation on iron-bearing dust solubility, *Atmos. Chem. Phys.*, *13*(9), 4895–4905, doi:10.5194/acp-13-4895-2013.

Paris, R., K. V. Desboeufs, and E. Journet (2011), Variability of dust iron solubility in atmospheric waters: Investigation of the role of oxalate organic complexation, *Atmos. Environ.*, *45*(36), 6510–6517, doi:10.1016/j.atmosenv.2011.08.068.

Plessow, K., K. Acker, H. Heinrichs, and D. Möller (2001), Time study of trace elements and major ions during two cloud events at the Mt. Brocken, *Atmos. Environ.*, *35*(2), 367–378.

Possner, A., E. Zubler, U. Lohmann, and C. Schär (2015), Real-case simulations of aerosol–cloud interactions in ship tracks over the Bay of Biscay, *Atmos. Chem. Phys.*, *15*(4), 2185–2201, doi:10.5194/acp-15-2185-2015.

Rosenfeld, D., S. Sherwood, R. Wood, and L. Donner (2014), Climate effects of aerosol-cloud interactions, *Science*, *343*(6169), 379–380, doi:10.1126/science.1247490.

Russell, L. M., et al. (2013), Eastern Pacific Emitted Aerosol Cloud Experiment, *Bull. Am. Meteorol. Soc.*, *94*(5), 709–729, doi:10.1175/bams-d-12-00015.1.

Scheinhardt, S., K. Müller, G. Spindler, and H. Herrmann (2013), Complexation of trace metals in size-segregated aerosol particles at nine sites in Germany, *Atmos. Environ.*, *74*, 102–109, doi:10.1016/j.atmosenv.2013.03.023.

Shi, Z., M. D. Krom, S. Bonneville, A. R. Baker, T. D. Jickells, and L. G. Benning (2009), Formation of iron nanoparticles and increase in iron reactivity in mineral dust during simulated cloud processing, *Environ. Sci. Technol.*, *43*(17), 6592–6596.

Siefert, R. L., A. M. Johansen, M. R. Hoffmann, and S. O. Pehkonen (1998), Measurements of trace metal (Fe, Cu, Mn, Cr) oxidation states in fog and stratus clouds, *J. Air Waste Manage.*, *48*(2), 128–143, doi:10.1080/10473289.1998.10463659.

Sorooshian, A., Z. Wang, M. M. Coggon, H. H. Jonsson, and B. Ervens (2013), Observations of sharp oxalate reductions in stratocumulus clouds at variable altitudes: Organic acid and metal measurements during the 2011 E-PEACE campaign, *Environ. Sci. Technol.*, *47*(14), 7747–7756, doi:10.1021/es4012383.

Straub, D. J., J. W. Hutchings, and P. Herckes (2012), Measurements of fog composition at a rural site, *Atmos. Environ.*, *47*, 195–205, doi:10.1016/j.atmosenv.2011.11.014.

Stumm, W. W., and J. J. Morgan (1996), *Aquatic Chemistry: Chemical Equilibria and Rates in Natural Waters*, 3rd ed., Wiley, New York.

Sun, L., Y. Wang, T. Yue, X. Yang, L. Xue, and W. Wang (2015), Evaluation of the behavior of clouds in a region of severe acid rain pollution in southern China: Species, complexes, and variations, *Environ. Sci. Pollut. Res.*, *22*(18), 14,280–14,290, doi:10.1007/s11356-015-4674-5.

Sun, M., Y. Wang, T. Wang, S. Fan, W. Wang, P. Li, J. Guo, and Y. Li (2010), Cloud and the corresponding precipitation chemistry in south China: Water-soluble components and pollution transport, *J. Geophys. Res.*, *115*, D22303, doi:10.1029/2010JD014315.

Tao, J., L. Zhang, G. Engling, R. Zhang, Y. Yang, J. Cao, C. Zhu, Q. Wang, and L. Luo (2013), Chemical composition of PM2.5 in an urban environment in Chengdu, China: Importance of springtime dust storms and biomass burning, *Atmos. Res.*, *122*, 270–283, doi:10.1016/j.atmosres.2012.11.004.

Travnikov, O., Ilyin, I., Rozovskaya, O., Varygina, M., Aas, W., Uggerud, H. T., Mareckova, K., and Wankmueller, R. (2012), Long-term changes of heavy metal transboundary pollution of the environment (1990–2010), EMEP Status report, 2/2012.

Unger, N., S. Menon, D. M. Koch, and D. T. Shindell (2009), Impacts of aerosol-cloud interactions on past and future changes in tropospheric composition, *Atmos. Chem. Phys.*, *9*(12), 4115–4129, doi:10.5194/acp-9-4115-2009.

Wang, G., J. Li, C. Cheng, S. Hu, M. Xie, S. Gao, B. Zhou, W. Dai, J. Cao, and Z. An (2011), Observation of atmospheric aerosols at Mt. Hua and Mt. Tai in central and east China during spring 2009—Part 1: EC, OC and inorganic ions, *Atmos. Chem. Phys.*, *11*(9), 4221–4235, doi:10.5194/acp-11-4221-2011.

Wang, Y., M. Sun, P. Li, Y. Li, L. Xue, and W. Wang (2011), Variation of low molecular weight organic acids in precipitation and cloudwater at high elevation in South China, *Atmos. Environ.*, *45*(36), 6518–6525, doi:10.1016/j.atmosenv.2011.08.064.

Wang, Z., A. Sorooshian, G. Prabhakar, M. M. Coggon, and H. H. Jonsson (2014), Impact of emissions from shipping, land, and the ocean on stratocumulus cloud water elemental composition during the 2011 E-PEACE field campaign, *Atmos. Environ.*, *89*, 570–580, doi:10.1016/j.atmosenv.2014.01.020.

Warneck, P. (1999), *Chemistry of the Natural Atmosphere*, 2nd ed., Academic Press, New York.

Weller, C., A. Tilgner, P. Brauer, and H. Herrmann (2014), Modeling the impact of iron-carboxylate photochemistry on radical budget and carboxylate degradation in cloud droplets and particles, *Environ. Sci. Technol.*, *48*(10), 5652–5659, doi:10.1021/es4056643.

Weschler, C. J., M. L. Mich, and T. E. Graedel (1986), Speciation, photosensitivity, and reactions of transition metal ions in atmospheric droplets, *J. Geophys. Res.*, *91*, 5189–5204, doi:10.1029/JD091iD04p05189.

Wong, M. S., F. Xiao, J. Nichol, J. Fung, J. Kim, J. Campbell, and P. W. Chan (2015), A multi-scale hybrid neural network retrieval model for dust storm detection, a study in Asia, *Atmos. Res.*, *158–159*, 89–106, doi:10.1016/j.atmosres.2015.02.006.

Yang, Y., Y. Wang, T. Wen, Y. Zhao, and J. Li (2009), Element characteristics and sources of $PM_{2.5}$ at Mount Dinghu in 2006, *Environ. Sci.*, *30*(4), 988–992.